
Article:
Tizani, W., Wang, Z.Y. and Hajirasouliha, I. (2012) Hysteretic performance of a new blind bolted connection to concrete filled columns under cyclic loading: An experimental investigation. Engineering Structures, 46. 535 - 546. ISSN 0141-0296

https://doi.org/10.1016/j.engstruct.2012.08.020

Tizani W, Wang ZY & Hajirasouliha I (2013) Hysteretic performance of a new blind bolted connection to concrete filled columns under cyclic loading: An experimental investigation. *Engineering Structures*, 46, 535-546.

Hysteretic Performance of a New Blind Bolted Connection to Concrete Filled Columns under Cyclic Loading: An Experimental Investigation

Walid Tizani*, Zhi Yu Wang and Iman Hajirasouliha
Department of Civil Engineering, The University of Nottingham, Nottingham, UK
* Corresponding author: Walid.Tizani@nottingham.ac.uk

ABSTRACT

The structural performance and reliability of a new blind-bolting technique is investigated in this study. The new blind-bolt is termed Extended Hollobolt (EHB) and is a modification of the standard Hollobolt. The EHB enhances the tensile resistance and stiffness of the fastener by anchoring it in the concrete infill of a tubular column. This paper reports on an investigation into the cyclic behaviour of end-plate connections to concrete filled tubular (CFT) columns using the EHB. A series of six full-scale connections were tested under quasi-static cyclic loading. The key parameters investigated were amplitude of cyclic loading procedure, bolt grade, tube wall thickness, and concrete grade. The strength, stiffness, rotation capacity and energy dissipation capacity of the connections were evaluated at different load cycles. In general, the EHB provided stable hysteretic behaviour with appropriate level of strength and stiffness. The influence of tube wall thickness and concrete grade on the strength, stiffness and failure mode of the connections is investigated. It is shown that sufficient performance can be achieved by controlling the tube wall thickness and concrete strength. The results indicate that the connection can offer energy dissipation capacity and ductility appropriate for its potential use in seismic design.

Keywords: Endplate connections; Blind bolts; Concrete filled tubes; Cyclic behaviour

1 INTRODUCTION

The advantages obtained by using concrete-filled tubes (CFT) in multi-storey construction have been recognised for a number of years [1]. Tubular sections are more efficient than open sections when dealing with compression, and their load carrying capacity can be significantly increased when filled with concrete. Moreover, the ductility and rotation capacity of the CFT columns is much enhanced when compared with

other types of composite columns, as the infill concrete is confined and cannot split away even if its ultimate strength is reached [2]. As a result, CFT columns are very attractive for seismic design of moment resisting frames in seismic zones. The connection to CFT columns, however, tends to be complicated and would normally involve welding [3] or the use of embedded steel bars [4] to develop sufficient moment capacity. The post-earthquake survey conducted following the Northridge earthquake 1994 indicated poor performance of welded beam to column connections, as they led to brittle fractures and catastrophic failures in steel structures [5]. As an alternative solution, some improved connection configurations have been suggested by contemporary researchers, such as bolted endplate connections, which is popular in Europe. This type of connection is also favoured since it involves shop welding and on-site bolting, thus avoids issues related to site welding. This type of connection is also available for tubular sections through the use of blind bolts (such as Hollbolt and Flowdrill), but only as simple pin connections resisting shear loads and some tension mainly to satisfy the integrity criterion [2]. Blind bolts are bolts that are only tightened from one side (more details are available from [6]).

Moment-resisting blind-bolted connections to hollow columns are not currently available in practice. However, a number of research studies have been conducted to determine the resistance of such systems mainly for typical connections (such as those using Hollbolt, Flowdrill Ajax One-side). Examples of these studies include work done to evaluate the tensile strength and stiffness of blind-bolt fasteners using T-stub models [1-9] and full scale endplate connections to CFT columns [10] and others experimental connections types [11, 12]. France et al [13] conducted monotonic loading tests on Flowdrill connections to CFT columns, and showed that the strength and stiffness of such connections are dramatically higher than those without concrete infill. Loh et al. [14] tested cruciform composite blind bolted endplate connections to CFT column under bending. They reported that using CFT prevents local tube failures. In contrast, hollow steel would typically fail by excessive deformation of tube face and pull out of the Hollobolts. Goldsworthy et al. [15] conducted tests on blind bolted T-stub connections. They used a modified Ajax one-side blind bolt. The modification involved welding a piece of steel reinforcing bar to the end of the bolt shank that was anchored in the concrete infill. Good results regarding failure modes and capacities were reported except for unexpected fractures in welds which occurred at the extension bars in some tests. In another study, Wang et al [16] performed monotonic and cyclic loading tests on eight cruciform bolted endplate connections with

Hollobolts. They used cold-formed tubes, which have affected the failure mode of the tubes from face bending to splitting at the corners (a typical failure mode for cold-formed tubes).

Tizani and Ridley-Ellis [9] performed investigation using a modified Hollobolt, called the Extended Hollobolt (EHB). In the EHB an extended bolt shank is used with an additional nut (called the anchor nut) as shown in Figure 1. The extended shank is immersed in the concrete infill and thus can provide an enhanced blind-bolt tensile strength and stiffness. This technique has proved to be very beneficial as the tensile failure mode of the EHB resembles that of the standard bolt-nut fastener (i.e the ultimate tensile resistance of the bolt shank is achieved through bolt shank fracture. This is compared with the typical failure mode of the standard Hollobolt, which is the pulling out of the connected tube by either the shear failure of its sleeve or the punching shear of the tube. This latter failure mode tends to occur at a lower resistance level compared to the ultimate resistance of the bolt shank.

Recent design guidelines, such as FEMA-350 [17] and Eurocode-8 [18], have incorporated the use of semi-rigid and/or partial strength connections. The performance of moment-resisting (semi-rigid to rigid) blind-bolted connections under cyclic loading has been investigated for top and bottom cleat connections made with Hollobolts [19] and for endplate connections to circular hollow sections using Ajax One-side blind bolts [15]. In these studies, the influences of relevant material and geometric parameters on the cyclic behaviour of the connections were examined.

Al-Mughairi et al. [10] reported significant improvement in the stiffness of endplate connections made with the EHB under monotonic loading where the connections exhibited rigid or semi-rigid behaviour. This outcome was encouraging for this type of connection. However, the performance of this type of blind-bolted connection under cyclic loading has not yet been examined.

The work presented in this paper attempts to address this issue by investigating the inelastic hysteretic behaviour of the new proposed blind-bolted connection. The expected response of such connection is more complex than those not involving concrete infill. This is due to the unknown contribution of the EHB anchorage in the concrete under cyclic loading. The current study involves conducting representative experimental programme to examine the contribution of the EHB, the confined concrete and the column face. Based on the experimental results, the cyclic characteristics of the blind-bolted connection using the EHB are presented and discussed in terms of failure modes, strength, stiffness, and energy dissipation.

2 EXPERIMENTAL PROGRAMME

2.1 Test Specimens

To study the hysteretic behaviour of the blind-bolted connections to CFT using the EHB, six full-scale beam to column connections have been tested under quasi-static cyclic loading. The connection detailing and the test arrangements are shown in Figure 2 and Figure 3, respectively. The following parameters were varied in the test specimens: tube wall thickness (tc), blind bolt grade (bgr), Concrete grade (cgr), and loading procedure (lp) (see Table 1). The specimens were designated as BBEC-tc-bgr-cgr-lp, where BBEC denotes blind-bolted-endplate-connection. For instance, the reference for Test 4 in Table 1, BBEC-5-8.8-50-LII, stands for a tested specimen using 5 mm thick tube, 8.8 blind bolt grade, and with nominal concrete strength of 50N/mm2, tested using cyclic loading procedure type II. The applied quasi-static cyclic loadings (type I and II) will be introduced in the next section. All test specimens were designed with similar configurations of steel beam (UB356×171×67 mm), endplate (404×220×25 mm) and 3 rows of bolts as shown in Figure 2. This configuration was determined to provide sufficient capacity and stiffness of the beam and endplate, thereby eliminating their influence on the joint failure mechanism. The design of the test specimens is outlined as follows: tests T1 and T2 to study the influence of bolt grade; tests T2 and T3 to study the influence of cyclic loading procedure; tests T1, T4 and T5 to study the influence of tube wall thickness; and tests T5 and T6 to study the influence of concrete strength.

The blind bolts used in the tests were 16mm diameter (M16) with extended shank length and an end anchor nut (Figure 1). The blind bolts were initially tightened with a spanner and then with a torque wrench in accordance to the specified torque values listed in Table 1. Prior to concrete casting and vibration, the anchor nut was prevented from unexpected rotation and removal by securing it using special glue. Standard concrete cubes were cast at the same time as the test specimens and cured in water at room temperature of approximately 20°C. The compressive strengths of the concrete cubes at the time of testing are summarized in Table 1. The material properties of the steel components are shown in Table 2. These values were obtained using tensile coupons designed and tested according to EN 10002-1: 2001 [20].

2.2 Experimental Test Set-up

Figure 2 and Figure 4 show the experimental test set-up used in this study. The specimens have been tested in the horizontal plan to lower the height of the actuator and reduce the loading demands on the reaction frames fixed on the strong floor (see Figure 4). The CFT column (d) was securely fastened into the test rig by roller supports positioned at both column ends to prevent any sideway and horizontal movements. To avoid the local crushing of concrete, two smooth plates were attached to the column ends in contact with the roller supports. To prevent uplift, the CFT column was laterally restraint (r) in the vicinity of the column ends by bolting to the anchorage points on the strong floor. As the face of the CFT column was expected to undergo local deformations induced by the blind bolt in tension, the connecting and sidewall faces of the CFT column were coated with a hydrated lime solution to help observing yield line patterns.

To develop bending moment at the blind bolted connection, a 450kN actuator (b) was rigidly bolted on a reaction buttress (c) to apply horizontal cyclic load to the steel beam (a) at 1.28m away from the column face. A linkage system was placed between the actuator and the test beam to accommodate the beam rotation. The rose joint at the end of the extension of the actuator was connected with a head cap (l) using a couple of rigid links (m). A sliding base carried by three pairs of horizontal rollers was used to carry the gravity loads. The effects of column axial loads on the hysteretic behaviour of the connections are not considered in this study, and therefore, no such loading was applied.

2.3 Instrumentation

A representative layout of the instrumentation adopted in the experimental tests is shown in Figure 2. The displacements of the steel beam, steel tube and endplate were measured using Linear Variable Differential Transformers (LVDTs) and potentiometers. These measurements were used to calculate the rotation of the connections. Strain measurements were collected from connecting and sidewall faces of the CFT column, the web and flange of the beam, and the face of the endplate as shown in Figure 2. The strain measurements on the face of the CFT column were collected in two directions parallel and perpendicular to the bolt row using two-elements cross strain gauges. Single-element strain gauges were placed on the side of the column (close to the corner) to monitor the highest strains on the sidewall surfaces. A number of blind bolt samples were also instrumented by flattening small areas to place strain gauges just beneath the bolt head and the anchored

nut. These instrumented bolts were considered to have reduced strength, and therefore, have been placed in the middle bolt row of the connection to avoid most highly loaded positions.

2.4 Joint Moment-Rotation Measurement

Considering the experimental setup shown in Figure 4, bending moments at the connections can be calculated as the applied force times the lever arm measured to the face of the CFT column. The bending moment was adjusted to take into account the horizontal component of the force when the angle of the applied load became significant [21]. The overall joint rotation was taken as the rigid body rotation of the beam relative to the column centreline. Figure 5 illustrates the measured rotations relative to the original column position. As shown in this figure, the joint rotation (θ_j) can be determined as the beam rotation (θ_o) minus the column rotation (θ_c). The beam elastic rotation was found to be negligible as the measurements were taken from the closest LVDTs to the CFT column. The following parameters have been calculated from the rotation measurements:

- **Initial stiffness:** The initial stiffness (K_e) of the connections was determined from the initial slope of the hysteresis curves.
- **Rotation Capacity:** The rotation capacity of the connections (θ_{peak}) was determined as the maximum rotation before failure.
- **Yield point:** The yield rotation of the connection was determined based on the FEMA-356 recommendations [22]. In this method, the hysteresis envelope curve is represented by a bilinear curve with a post-yield slope (αK_e) as shown in Figure 6. The yield rotation (θ_y) is determined on the condition that the secant slope intersects the actual envelope curve at 60% of the nominal yield moment (M_y), while the area enclosed by the bilinear curve is equal to that enclosed by the original curve bounded by the peak rotation (θ_{peak}).

2.5 Quasi-Static Cyclic Loading Procedure

For this testing programme, the loading procedure suggested by the European Convention for Constructional Steelwork ECCS [23], was adopted as summarised in Figure 7. In this figure, δ is the applied displacement and δ_y is the estimated yield displacement. The loading procedure involves applying at least four levels of displacements before attaining the joint yielding displacement (δ_y) and then applying a set of 3

cycles at each displacement level. The displacement levels are determined by increasing the displacement by a pre-determined increment. The increments used in this study were $0.5\delta_y$ (Procedure I: δ_y, $1.5\delta_y$, $2\delta_y$, $2.5\delta_y$, $3\delta_y$, $3.5\delta_y$, ...) and $2\delta_y$ (Procedure II: δ_y, $2\delta_y$, $4\delta_y$, $6\delta_y$, $8\delta_y$, ...). Procedure I was used for the test specimens T1 and T2, while the loading procedure II was adopted for the rest of the test specimens.

3 EXPERIMENTAL RESULTS AND OBSERVATIONS

The observed physical damage and the main response parameters obtained from the experimental tests are presented and discussed in this section.

3.1 Failure Modes

The cyclic characteristics of the connections in this study were substantially dependent on the failure mechanisms of the blind bolt and the CFT column. Therefore, the influence of material properties and geometric parameters on the failure mechanisms of the blind bolt and the CFT column was investigated in the test programme. As it was mentioned before, the steel beam and the endplate elements were relatively strong to avoid influencing the failure mode of the connections. During the cyclic loading process, the observed physical damage was recorded at each load step. Typical failure modes observed in the experimental tests are illustrated in Figure 8. Based on the results, the following two different failure modes were identified:

- **Failure mode I**: bolt shank facture with limited tube face yielding. In this case the bolt shank elongation acts as the primary source of deformation, and the CFT column has relatively higher strength and stiffness compared to the blind bolt (i.e., thick tube face and/or high strength concrete infill). This connection category is labelled as ‘weak blind bolt - strong CFT column’. Test T2 is taken as representative of failure mode I.
- **Failure mode II**: moderate deformation of CFT column face, local damage to concrete infill and partial bolt pull-out with likely local cracking in the bolt sleeves. In this case, the blind bolt assembly undergoes greater deformation and the CFT column exhibits relatively weaker strength and stiffness compared to the blind bolt (i.e., relatively thin tube face and/or low strength concrete infill). The connection category in this case is labelled as ‘strong blind bolt - weak CFT column’. Test T4 is taken as representative of the failure mode II.

As a general observation, the tests T1, T2, T3 and T5 failed by mode I, while T4 and T6 failed by mode II (see Figure 8). Tests with failure mode I had column wall thickness of equal to or greater than 6.3 mm, and nominal concrete grade of 50 N/mm^2. Tests with failure mode II had either column wall thickness of less than 6.3 mm or nominal concrete strength of lower than 50 N/mm2.

To examine the failure mechanism of the CFT column, the connections were dismantled first by cutting off the heads of the bolts which did not fail and by removing the steel beam and the endplate. Subsequently, a strip of the tube was cut to reveal the condition of the concrete infill (see Figure 8).

For the connections that failed in mode I, the endplate rotated as a rigid body about the compression flange of the beam (Figure 8 (a)), while the column remained almost rigid. In this case, the gap between the endplate and the CFT column is linear, and thus results in a linear distribution of forces to the bolt rows corresponding to their distance from the rotation point. The deformations on the CFT column connecting face and sidewall face were almost invisible, but the local yielding patterns were revealed against the hydrated lime solution on the corners of the tube connecting face. This was especially apparent at outer bolt rows which attracted the highest forces (Figure 8 (c)). The concrete infill in this failure mode (mode I) remained intact except for a local crushing about the bolt clearance holes where the blind bolts were pulled outwards (Figure 8 (e)). This suggests that the concrete infill efficiently restrained the blind bolt from pulling out, thereby forcing the bolt shank fracture failure.

For the connections that failed in mode II, in contrast, the CFT column connecting face at the first and second bolt rows deformed significantly with partial bolt pull-out, resulting in a very small gap between the endplate and the column. While excessive deformation of the column face was observed, the blind bolts did not show any sign of bolt shank fracture. The connection face of the CFT column exhibited visible flexible deformations at each bolt row with yield patterns developed around the bolt clearance holes. These yield patterns were extended to the corners between the connecting face and the sidewall. In the failure mode II, greater local concrete crushing and widespread concrete damage in the connection regions were observed. After cleaning the loose concrete, it was evident that the local concrete is crushed not only near the anchor nut but also along the bolt shank which implies significant loss of anchorage and bond for the blind bolts at large rotations (Figure 8 (f)).

The blind bolts failed in the mode I are featured by the bolt shanks rupture with the bolt heads stripped at the outer bolt row (see Figure 8 (g)). The bolt shank rupture located approximately 15mm~28mm from the bottom surface of the bolt head, which is expected to be within the bolt clamping length. All of the bolt shanks in this case exhibited very limited necking, which demonstrates a brittle rupture rather than a ductile failure pattern. It was also observed that the rubber washers were almost squashed in contact with the bottom bolt head. This implies that the mechanical interlock between the blind threaded cone bolt and sleeve still remained effective up to the bolt shank rupture.

In the failure mode II, no noticeable damage was observed in the blind bolts at the interlocked assembly part and the bolt shank anchored in the concrete infill (see Figure 8 (h)). However, small local cracks, initiated from the slots between the flaring sleeves, were observed in the straight portion of the sleeves. This could be explained by the fact that the interlocked threaded cone is more prone to over-squeeze the flaring sleeve whilst the connection is subjected to large rotations. The bolt shanks at this stage should be able to carry a certain level of tensile loads, as the tensile deformations are shared by the flexibility of the tube connecting face rather than dependent on the bolt shank elongation solely.

4 HYSTERESIS BEHAVIOUR OF THE CONNECTIONS

4.1 Moment-Rotation Curves

The moment-rotation relationship is the principle means of evaluating and characterising the behaviour of beam-to-column connections. The hysteretic moment-rotation curves of the tested connections are shown in Figure 9. The key characteristics of the connection, such as moment capacity, rotation capacity and initial stiffness are summarized in Table 3.

Figure 9 (a), (b), (c), and (e) show the hysteretic moment-rotation curves for the tests T1, T2, T3, and T5 that all failed in the mode I (i.e. bolt fracture). The hysteretic curves for these tests exhibit minor pinching. The rotation increment along zero moment axis of loading and unloading excursions indicates that the joint rotation is governed by the bolt shank elongation or slip rather than the plate flexibility. This is because this rotation was not accompanied by noticeable load increment. Moreover, it is noted that the areas enclosed by the cyclic excursion of the first loading cycle for each displacement level are slightly larger than those generated by subsequent cycles. This observation will be discussed in more detail in the following section.

Figure 9 (d) and (f) show the hysteretic curves for the T4 and T6 tests with failure mode II (i.e. flexible column face deformation). The shape of the hysteretic moment-rotation curves for these tests is relatively similar to that for the connection category I until the maximum moment is reached. However, their hysteretic moment-rotation behaviour exhibited significant pinching and higher load deterioration under subsequent cyclic loading. It is shown that, for T4 and T6 tests, the maximum moment capacity and the areas enclosed by the cyclic excursions are increasingly reduced as the joint rotation becomes larger. This behaviour can be attributed to the progressive concrete crushing in the failure mode II as discussed before.

The envelope of moment-rotation hysteretic curves for different test specimens is compared in Figure 10. This figure shows that the behaviour of the proposed blind bolted endplate connection under cyclic loading was mainly influenced by the failure mode of the connections. It is demonstrated that the connections with failure mode I (T1, T2, T3 and T5) could undergo rotations slightly greater than 25 mrad, with a reduction in strength of less than 20%, which is suitable for the connections in frames of medium ductility class (DCM) according to Eurocode-8 [18]. On the other hand, the connections with failure mode II (T4 and T6) exhibited rotation capacity significantly larger than 35 mrad (up to 93 mrad), with less than 20% reduction in strength, that is ideal for the moment resisting frames designed for high ductility class (DCH) [18]. The ductility characteristics of the proposed connections will be discussed in more details in the following sections.

4.2 Effects of Key Design Variables

In this study, the influence of the bolt-grade, loading procedure, tube wall slenderness, and concrete strength on the hysteretic behaviour of the proposed blind-bolted connection is investigated. Based on the experimental results, the following conclusions can be made:

Blind bolt grade: Figure 10 (a) illustrates the influence of the blind bolt grade on the moment-rotation relationship of the connections by comparison between the behaviour of T1 (8.8 bolt grade) and T2 (10.9 bolt grade) specimens. The results indicate that the use of higher blind bolt grade in the T2 specimen resulted in an almost 20% increase in the moment of resistance and initial stiffness, but slightly reduced the rotation capacity of the connection compared with the T1 specimen (data in Table 3). This observation was expected as the blind bolt grade affects both the bolt tensile strength and the preload with beneficial effects on the strength and stiffness of the connection.

Cyclic loading procedure: The influence of the loading procedure is studied by comparison between the hysteretic envelope curves of T2 (loading procedure L1) and T3 (loading procedure L2) tests as shown in Figure 10 (b). The results indicate that both envelopes are in close agreement in terms of strength, stiffness and rotation capacity in the positive excursion. There is a slight difference, however, in the negative excursion where using smaller displacement increment in T2 has resulted in a slightly higher ultimate rotation. The results, in general, indicate that the loading procedure does not affect the overall hysteric behaviour of the tested specimens.

Tube wall slenderness: The tube wall slenderness ratio is expected to directly influence the strength and flexibility of the CFT column face. The influence of tube wall slenderness is studied by comparison between the hysteretic behaviour of T4 (5 mm thick tube), T5 (6.3 mm thick tube) and T1 (8 mm thick tube) specimens as shown in Figure 9 (d), (e) and (a), respectively. The slenderness ratio in these specimens are varied by changing the tube thickness while maintaining the tube width. For better comparison, the moment-rotation envelope curves of the samples with different slenderness ratio are given in Figure 10 (c). It can be observed that the tube wall slenderness can influence the initial stiffness of the connections (up to 30%). However, the results indicate that the strength and rotation capacity of the connections mainly depend on the failure mode. For example, it is shown in Figure 10 (c) that changing the tube thickness from 8 to 6.3 mm did not influence the strength and ultimate rotation of the connections as both samples failed in mode I (i.e. bolt fracture). However, the initial stiffness of the thicker tube was 23% higher. The failure mode of the connection was changed from mode I (in T1 and T5) to mode II (in T4) as a result of reducing the tube thickness to 5 mm. This implies that beyond a certain slenderness limit the concrete infill will be more prone to damage. This can weaken the blind bolt anchorage in tension, and therefore, reduce the strength of the connection. It is suggested that the use of relatively thin tubes prevented the connection from utilising the full potential strength of the blind-bolt, and as a result, reduced the connection strength and stiffness. However, the rotational capacity of the connection with slender tube wall (T4 specimen) was greatly improved due to its ductile failure mode (failure mode II).

Concrete grade: The concrete infill can provide confinement for the tube, and anchorage for the blind-bolt. It was originally thought that the concrete strength would not be a major factor as low strength concrete could still provide sufficient confinement effects. However, the test results showed that the concrete strength

can significantly affect the behaviour of CFT columns with relatively high tube wall slenderness ratio. The influence of the concrete compressive strength can be observed by comparison between the hysteretic behaviour of tests T5 (concrete strength of 53 N/mm^2) and T6 (concrete strength of 21 N/mm^2) as shown in Figure 9 (e) and (f) and Figure 10 (d). It is immediately apparent that the concrete strength has influenced the failure mode of the connections (mode I in T6 and mode II in T5). Using low strength concrete resulted in a 17% reduction in the rotation capacity, 18% reduction in the initial stiffness, and 260% increase in the rotation capacity as the failure mode changed from type I (i.e. bolt fracture) to type II (i.e. flexible column face deformation). It is clear from the results that the low strength concrete led to the failure of bolt anchorage, and as a result the tensile stiffness of the blind-bolt was controlled by the tube-wall alone. This was confirmed by inspecting the failed samples (Figure 8) where it is observed that the concrete anchorage was hardly damaged for failure mode I (T5 specimen) but it was completely crushed for samples with failure mode II (T4 and T6 specimens). It is also worth noting that the overall behaviour of the weak-concrete connection (T5) is comparable to that of the relatively weak tube wall connection (T4) with the exception of the ultimate moment strength.

5 CYCLIC CHARACTERISTICS OF THE CONNECTIONS

The cyclic performance of the connections with different material and geometric parameters are evaluated and discussed in this section. The assessment is based on the data obtained from tests T1 and T2, as representatives of failure mode I (i.e. bolt fracture), and T4 and T6, as representatives of connections with failure mode II (i.e. flexible column face deformation).

5.1 Key Performance Parameters

The performance parameters studied in this study are strength and stiffness degradation, ductility, and energy dissipation ratio based on the ECCS [23] and ATC [24] recommendations. Brief definitions of these parameters are given below and the symbols are described in Table 4 and Table 5.

Ductility: Ductility is defined as the ability of the structure to undergo large plastic deformation without significant loss of strength [25]. The concept of ductility is a key element in earthquake-resistant design of structures. The assessment of ductility for connections can be carried out by calculating partial ductility (μ_{0i}) and full ductility ratio (μ_{fi}) as defined in Table 5. The partial ductility indicates the capability of the

connection to accept nonlinear rotations without extensive damage, while the full ductility ratio is a parameter to describe the moment-rotation relationship of the connection at i^{th} excursion.

Strength ratio: Strength (or resistance) ratio is an important parameter to evaluate the performance of connections under dynamic/cyclic loadings such as earthquake ground motions. Strength deterioration is evaluated using the strength ratio, α_{ri}, which is the ratio of the moment at peak rotation to the initial yield moment, as given in Table 5.

Stiffness degradation: Connections with large degree of stiffness degradation tend to exhibit larger rotations under cyclic loads that may lead to extensive damage to other structural elements. Stiffness (or rigidity) degradation, ξ, is defined as the ratio of the secant stiffness at excursion i, $K_{s,i}$, to the initial stiffness, K_e (see Table 5).

Energy dissipation: The inelastic deformation of the connections aids to dissipate some energy through hysteretic behaviour, thereby reducing the transmitted energy to other structural elements. This can help to improve the seismic performance of the whole structural system under strong earthquakes. The energy dissipation capacity of the connection can be identified as the summation of the areas enclosed by hysteresis loops. The energy dissipation ratio, η_i, is defined as the ratio of the area enclosed by i^{th} cycle (either the positive or negative excursion) to the area formed by the yield moment and positive and negative excursions (see Table 5 for the full equation).

5.2 Performance Evaluation of the Connections

The efficiency of the proposed blind bolted endplate connections under cyclic loading is investigated by evaluating the performance parameters defined in the previous section at different load levels. The variation of full ductility ratio (μ_f), strength degradation ratio (α_r), stiffness degradation ratio (ξ), and energy dissipation ratio (η) versus partial ductility (μ_0) is calculated for the test specimens T1, T2, T4 and T6 as shown in Figure 11. The partial ductility factor in this figure can be representative of the cyclic loading ranging from yield point (i.e. μ_0 =1) to the failure point. The plots in Figure 11 are only for the positive excursions as those of the negative excursions exhibited similar characteristics. The hysteretic performance of the test specimens are evaluated and discussed in the following sections.

5.2.1 Connection Ductility

As it was expected, T4 and T6 specimens with the failure mode II (i.e. flexible column face deformation) exhibited significantly higher ductility compared to T1 and T2 specimens with the failure mode I (i.e. bolt fracture). The results shown in Figure 11 indicate that the partial ductility factor for the connections failed by mode I and mode II was on average 2.7 (i.e. medium ductility class) and 6.1 (high ductility class), respectively. This is in agreement with the classifications based on plastic rotation capacity as discussed in section 4.1.

Comparison of partial ductility and full ductility ratios for different test specimens in Figure 11 shows an almost identical behaviour for the specimens with similar failure modes. This implies that the ductility of the blind bolted endplate connections to CFT columns was mainly influenced by the failure mode rather than other design variables. It is shown in Figure 11 (a) and (b) that the full ductility ratio of T1 and T2 specimens had an almost linear descending tendency up to the failure point, which indicates a modest deterioration of the hysteresis loops in the connections with type I failure. Figure 11 (c) and (d) show a steep drop in the full ductility ratio of T4 and T6 specimens after the first set of cycles with an almost level performance beyond that. The sudden reduction can be attributed to partial or full failure of the bolt embedment in the concrete that would change the joint rotational resistance mechanism from tension in the bolt to simultaneous local concrete crushing and face bending. Beyond the second set of load cycles, there is a slight deterioration in the ductility performance of the T4 and T6 connections. This indicates that this connection category (limited by the face bending failure mode) has much larger rotational capacity compared to the connections with bolt-controlled failure mode.

5.2.2 Strength Ratio

Comparison of the strength ratios in Figure 11 indicates that samples with similar failure modes exhibited very similar behaviour. This emphasises the dominant role of the failure modes on the hysteretic behaviour of the connections. Figure 11 (a) and (b), show an improved resistance (relative to the yield strength) for T1 and T2 specimens, with failure mode I, up to the failure point. The only moderate degradation of strength was between successive cycles of the same amplitude, and no overall significant strength degradation was noticed before failure.

As shown in Figure 11 (c) and (d), the strength ratio of T4 and T6 specimens, with failure mode II, showed an initial improvement in the 2nd set of load cycles but afterwards it gradually degraded up to the failure point. Noticeable strength degradations were recorded between the successive cycles within the same load amplitude. This is can be attributed to the progressive crushing of concrete and loss of bolt anchorage under repeated cyclic loads. Overall, strength degradation of this type of blind bolted endplate connection to CFT column was not considered significant for both of the failure mode categories.

5.2.3 Stiffness Degradation

It is shown in Figure 11 that, similar to the other performance parameters, connections with similar failure modes have almost identical stiffness degradation behaviours. Figure 11 (a) and (b) show that the stiffness (or rigidity) degradation for the specimens with the failure mode I (i.e. T1 and T2) is decreased almost linearly from the 3rd sets of cycles up to the failure point. The results demonstrate a larger rate of deterioration of stiffness compared with strength and ductility.

The stiffness degradation ratios shown in Figure 11 (c) and (d) indicate a steep drop after the first set of cycles in the specimens with the failure mode II (i.e. T4 and T6). As explained earlier, these reductions can be attributed to the failure of the bolt embedment in the concrete and the subsequent changes in the joint rotational resistance. The results also show a noticeable degradation in the stiffness of T4 and T6 connections after the 2nd set of cycles. Beyond that, there is a gradual almost linear deterioration in the stiffness of the connections up to the failure point, where the stiffness ratio tends to zero.

It can be concluded that the stiffness degradation is more significant for the connections with failure due to the flexible column face deformation (mode II) compared to those with the bolt fracture failure (mode I). This can be easily explained as the loss of the bolt anchorage in the failure mode II has a significant effect on the stiffness of the connection, and also the contribution of the concrete infill to the stiffness is reduced as a result of extensive damage to the concrete. In general, it is shown that the stiffness degradation in the proposed blind bolted endplate connection is more significant than the degradation of strength and ductility.

5.2.4 Energy Dissipation

The energy dissipation ratio of the test specimens are compared in Figure 11. As it was expected, the energy dissipation of the connections reduced by increasing the load amplitudes (or cycles) up to the failure point. Similar to the previous performance parameters, the failure mode of the connections was the key

element for determining their energy dissipation capacity. In general, connections with failure mode II demonstrated higher energy dissipation ratio.

Figure 11 (a) and (b) show a significant drop in the energy dissipation capacity of T1 and T2 specimens (failure mode I) after the first cycle of loading. Beyond this point, a gradual decrease is noticed until the failure point. Similarly, Figure 11 (c) and (d) show a steep drop in the energy dissipation ratio of T4 and T6 specimens (failure mode II) after the first set of cycles with almost gradual descending performance beyond that. For both categories of connections, there was a dramatic drop of the absorbed energy ratio subsequent to the first cycle of each loading amplitude, which implies the absorbed energy reduces significantly during the repeated cycles. However, it can be observed that the amount of such reduction is reduced as the cyclic loading proceeds. This phenomenon can be explained by the fact that after a few cycles the energy is mainly dissipated by flexible deformation of the tube connecting face (as a plate element), rather than the sole action of the blind bolt in tensile deformation.

The results of this study indicate that the new blind bolted endplate connection to CFT column, in general, can offer good energy dissipation capacity and ductility which makes it suitable for seismic applications. It is particularly true for the connections in category II (failure due to flexible column face deformation) that exhibit high ductility and relatively low strength degradation under cyclic loading. In practice, the seismic performance of this type of connections can be significantly improved by controlling their failure mode in the design process (for example by using relatively thin tube face and/or low strength concrete). The experimental results and related analysis presented in this paper can be taken as a basic reference for the efficient design of this innovative blind bolted endplate connection to CFT columns. Development of detailed finite element and analytical macro models to simulate the hysteretic moment-rotation relationship of this type of connection will be discussed in a companion paper.

6 SUMMARY AND CONCLUSIONS

A series of six full-scale tests were conducted on a new blind bolted endplate connection to CFT columns using EHB under quasi-static cyclic loading. The strength, stiffness degradation, ductility, rotation capacity and energy dissipation of the connections were evaluated in relation to different material and geometric parameters. The primary results can be summarized as follows:

(1) The test observations indicate two representative failure modes. In failure mode I, described as weak blind bolt-strong CFT column, the bolt shank fractured ultimately with limited CFT column face yielding. In failure mode II, described as strong blind bolt- weak CFT column, the CFT column face deformed in a flexible manner with local damage of concrete infill and partial bolt pull-out. Connections with failure mode II exhibited significantly higher rotation capacity and ductility compared to those with failure mode I.

(2) During the cyclic loading tests, no damage was observed on the extension of the blind bolts. This suggests that the proposed bolt can provide stable improvement in strength and stiffness of the connection as long as the surrounded concrete is not crushed along the anchor nut.

(3) The strength, stiffness, and rotation capacity of the connections are rather insensitive to the loading amplitude of the cyclic loading procedure. The use of higher bolt grade increases the maximum strength and initial stiffness of the connections, but slightly reduces the counterpart rotation capacity. Any decrease in tube wall thickness and concrete grade is normally accompanied by a decrease in the strength and stiffness of the connection. However, this can change the failure mechanism of the connection from mode I to mode II which leads to a significant increase in the ultimate rotation and ductility.

(4) It is shown that the overall performance of the blind bolted endplate connections was mainly influenced by their failure mode. In general, connections with failure mode II (strong blind bolt- weak CFT column) demonstrated high energy dissipation and ductility ratio, and therefore, can be used in moment-resisting frames designed for high ductility class (HDC) that are suitable for high seismic zones.

7 ACKNOWLEDGEMENTS

The authors would like to thank Mr. Trevor Mustard and Mr. Andrew Orton of Tata Steel (formerly known as Corus) and Mr Neil F. Gill of Lindapter International for supporting this work. The second author would like to acknowledge financial support from 'UK/China Scholarship for Excellence' programme for his doctoral research work.

REFERENCES

1. Bergmann R, Matsui C, Meinsma C, Dutta D. Design Guide for Concrete Filled Section Columns under static and Seismic Loading. CIDECT. 1995.
2. Kurobane Y, Packer JA, Wardenier J, Yeomans N., Design Guide for Structural Hollow Section Column Connections. CIDECT and Verlag TüV Rheinland GmbH, Koln, Germany, 2004.
3. Alostaz YM, Schneider SP., Analytical behavior of connections to concrete-filled steel tubes. Journal of Constructional Steel Research. 1996(40): 95-127
4. Schneider SP, Alostaz YM., Experimental behavior of connections to concrete-filled steel tubes. Journal of Constructional Steel Research. 1998(45): 321-352

5. Mahin SA., Lessons from damage to steel buildings during the Northridge earthquake. Engineering Structures, 20(4-6), 1998: 261-270
6. Barnett, T.C., Tizani, W. and Nethercot, D.A., 2001. The practice of blind bolting connections to structure hollow sections - a review Steel and Composite Structures. 1(1), 1-16
7. Ellison S, Tizani W., Behaviour of blind bolted connections to concrete filled hollow sections. The Structual Engineer, November, 2004: 16-17
8. Wang ZY, Tizani W, Wang QY., Strength and initial stiffness of a blind-bolt connection based on the T-stub model, Engineering Structures, 32(9), 2010: 2505-2517
9. Tizani.W, Ridley-Ellis.D.J. The performance of a new blind-bolt for moment-resisting connections. In: Jaurietta MA, Alonso A, Chica JA, editors. Tubular structures X: Proceedings of the 10th international symposium on tubular structures. Rotterdam: A. A. Balkema, 2003: 395-400
10. Al-Mughairi, A, Tizani, W And Owen, J S, 2010. Validation Of An FE Model For An Experimental Blind-Bolted Moment-Resisting Connection To Concrete Filled Hollow Section
11. Elghazouli AY, et al. Experimental monotonic and cyclic behaviour of blind-bolted angle connections. Engineering Structures (2009), Volume 31, Issue 11, November 2009, Pages 2540–2553, doi:10.1016/j.engstruct.2009.05.021
12. Gardner, A.P.; Goldsworthy, H.M., Experimental investigation of the stiffness of critical components in a moment-resisting composite connection. Journal of Constructional Steel Research vol. 61 issue 5 May, 2005. p. 709-726, DOI: 10.1016/j.jcsr.2004.11.004. ISSN: 0143-974X.
13. France JE, Davison JB, Kirby PA., Strength and rotational response of moment connections to tubular columns using flowdrill connectors. Journal of Constructional Steel Research, 50(1), 1999: 35-48
14. Loh HY, Uy B, Bradford MA., The effects of partial shear connection in composite flush end plate joints Part I- experimental study. Journal of Constructional Steel Research, 62(4), 2006: 378-390
15. Goldsworthy H, Gardner AP., Feasibility study for blind bolted connections to concrete-filled circular steel tubular columns. Structural Engineering and Mechanics, 24(4), 2006: 463-478
16. Wang JF, Chen XY, Han LH., Structural behaviour of blind bolted connection to concrete-filled steel tubular columns. Advanced Material Research, 163-167, 2011: 591-595
17. FEMA(350), Recommended seismic design criteria for new steel moment frame buildings. SAC Joint Venture, Federal Emergency Management Agency, Washington D.C, 2000
18. Eurocode 8: Design of structures for earthquake resistance - Part 1: General rules, seismic actions. BS EN 1998-1:2004, British Standard Institute, January 2011
19. Elghazouli AY, Málaga-Chuquitaype C, Castro JM, Orton AH., Experimental monotonic and cyclic behaviour of blind-bolted angle connections. Engineering Structures, Vol. 31(11), 2009:2540-2553
20. EN 10002-1, Metallic materials: tensile testing, Part 1: Method of test at ambient temperature. London: British Standards Institution, 2001
21. Wang ZY., Hysteretic response of an innovative blind bolted endplate connection to concrete filled tubular column. PhD Thesis, University of Nottingham, United Kingdom, 2012
22. FEMA 356, Prestandard and Commentary for the Seismic Rehabilitation of Buildings, Federal Emergency Management Agency, November, 2000
23. ECCS. Technical Committee 1:structutal safety and loadings: technical working group 1.3:seismic design, recommended testing procedure for assessing the behaviour of structural steel elements under cyclic loads, 1986
24. Guidelines for Cyclic Testing of Components of Steel Structures, ATC Applied Technology Council, ATC-24, 1992
25. Mazzolani FM., Moment resistant connections of steel frames in seismic areas. E&FN SPON Press. 2000: 95-96

Table 1. Details of test specimens.

Test No.	Specimen reference BBEC-t_c-b_{gr}-c_{gr}-l_p	SHS column section		Blind bolt		Concrete
		Nominal $b_c \times b_c \times t_0$ (mm)	Actual $b_c \times b_c \times t_0$ (mm)	Bolt grade	Tightening torque (Nm)	Strength (N/mm^2)
1	BBEC-8-8.8-50-LI	200×200×8	201.5×201.5×7.91	8.8	190	53.20
2	BBEC-8-10.9-50-LI	200×200×8	201.5×201.5×7.91	10.9	300	47.40
3	BBEC-8-10.9-50-LII	200×200×8	201.5×201.5×7.91	10.9	300	51.55
4	BBEC-5-8.8-50-LII	200×200×5	201.2×201.2×4.92	8.8	190	49.13
5	BBEC-6.3-8.8-50-LII	200×200×6.3	201.1×201.1×6.27	8.8	190	52.75
6	BBEC-6.3-8.8-25-LII	200×200×6.3	201.1×201.1×6.27	8.8	190	20.77

Note: Connecting steel beam size: UB 356×171×67, endplate size (mm): 404×220×25, blind bolt size: M16.

Table 2. Properties of steel components

Steel components		Yield strength (MPa)	Ultimate strength (MPa)	Elastic modulus (MPa)
Beam & endplate		500.20	581.18	194205
SHS tube	5mm	433.05	522.10	197194
	6.3mm	423.23	514.59	190512
	8mm	435.05	510.68	199114
Bolt shank	8.8 grade	752.33	918.18	194204
	10.9 grade	883.43	1112.32	209722
Bolt Sleeve		449.40	584.33	208830

Table 3. Summary of main results

Test No.	Yield point				Maximum moment point				Peak rotation point				Initial stiffness (KN.m/mrad)		Failure modes
	Yield moment (kN.m)		Yield rotation (mrad)		Moment (kN.m)		Rotation (mrad)		Moment (kN.m)		Rotation (mrad)				
	M_y^-	M_y^+	θ_y^-	θ_y^+	M_{max}^-	M_{max}^+	$\theta_{m,max}^-$	$\theta_{m,max}^+$	$M_{r,peak}^-$	$M_{r,peak}^+$	θ_{peak}^-	θ_{peak}^+	K_{ini}^-	K_{ini}^+	
T1	120.7	154.0	12.4	12.1	133.8	163.9	30.6	27.3	130.8	161.8	31.3	32.2	16.9	23.5	I
T2	149.0	173.0	12.0	11.3	164.7	189.0	22.3	21.8	154.6	166.4	36.7	34.9	20.1	27.1	I
T3	151.1	177.0	11.9	11.2	171.9	189.2	29.4	27.7	156.9	180.1	29.8	31.6	20.2	28.6	I
T4	107.2	132.5	15.5	14.4	115.8	157.7	32.1	30.5	62.2	116.7	77.2	86.5	14.1	18.0	II
T5	116.5	144.8	13.5	13.1	120.4	161.0	31.1	30.3	108.9	147.5	32.3	35.7	15.8	19.2	I
T6	97.1	121.2	15.4	14.9	103.0	137.3	30.6	30.4	64.6	110.2	83.3	92.8	13.7	16.2	II

+ or – denotes positive or negative excursion

Table 4. Definition of cyclic parameters [23, 24]

	Symbols	Definition
Moment	M_y^+, M_y^-	Yield moment based on envelop curve
	M_i^+, M_i^-	Moment at peak rotation in excursion *i*+ & *i*-
Rotation	θ_y^+, θ_y^-	Yield rotation in first excursion
	θ_i^+, θ_i^-	Peak rotation in excursion *i*+ & *i*-
	$\Delta\theta_{i+}$, $\Delta\theta_{i-}$	Rotation range from θ_y to the max in excursion *i*+ & *i*-
Stiffness	$K_{s,i}^+$, $K_{s,i}^-$	The secant slope of M-θ diagram at excursion *i*+ & *i*-
	K_e^+, K_e^-	Initial stiffness of M-θ diagram at the start
Energy	A_i^+, A_i^-	Area enclosed by hysteresis loops for excursions *i*+ & *i*-

Table 5. Definition of cyclic characterising parameters [23, 24]

Cyclic characterizing parameters	Symbol	Expressions
Partial ductility	μ_{0i}	θ_i^+/θ_y^+, θ_i^-/θ_y^-
Full ductility ratio	μ_{fi}	$\Delta\theta_{i+}/(\theta_i^+ + \theta_i^- - \theta_y^-)$, $\Delta\theta_{i-}/(\theta_i^+ + \theta_i^- - \theta_y^+)$
Strength or resistance ratio	α_{ri}	M_i^+/M_y^+, M_i^-/M_y^-
Stiffness degradation ratio	ξ_i	$K_{s,i}^+/K_e^+$, $K_{s,i}^-/K_e^-$
Energy dissipation ratio	η_i	$A_i^+/[M_y^+(\theta_i^+ - \theta_y^+ + \theta_i^- - \theta_y^-)]$ $A_i^-/[M_y^-(\theta_i^- - \theta_y^- + \theta_i^+ - \theta_y^+)]$

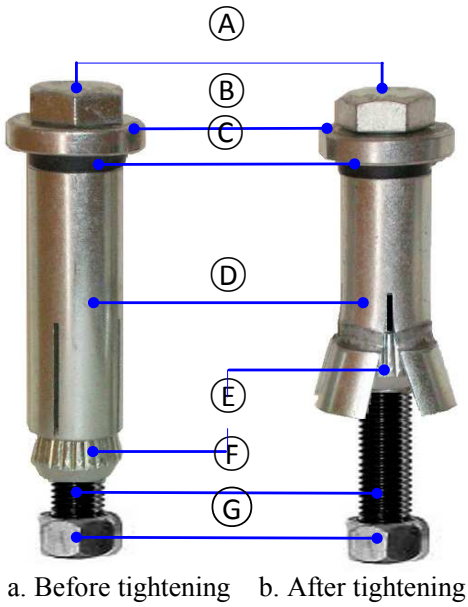

a. Before tightening b. After tightening

No.	Components
A	Bolt head
B	Collar
C	Rubber washer
D	Sleeve
E	Threaded cone
F	Bolt shank
G	Anchor nut

Figure 1. Components of the proposed Extended Hollobolt (EHB).

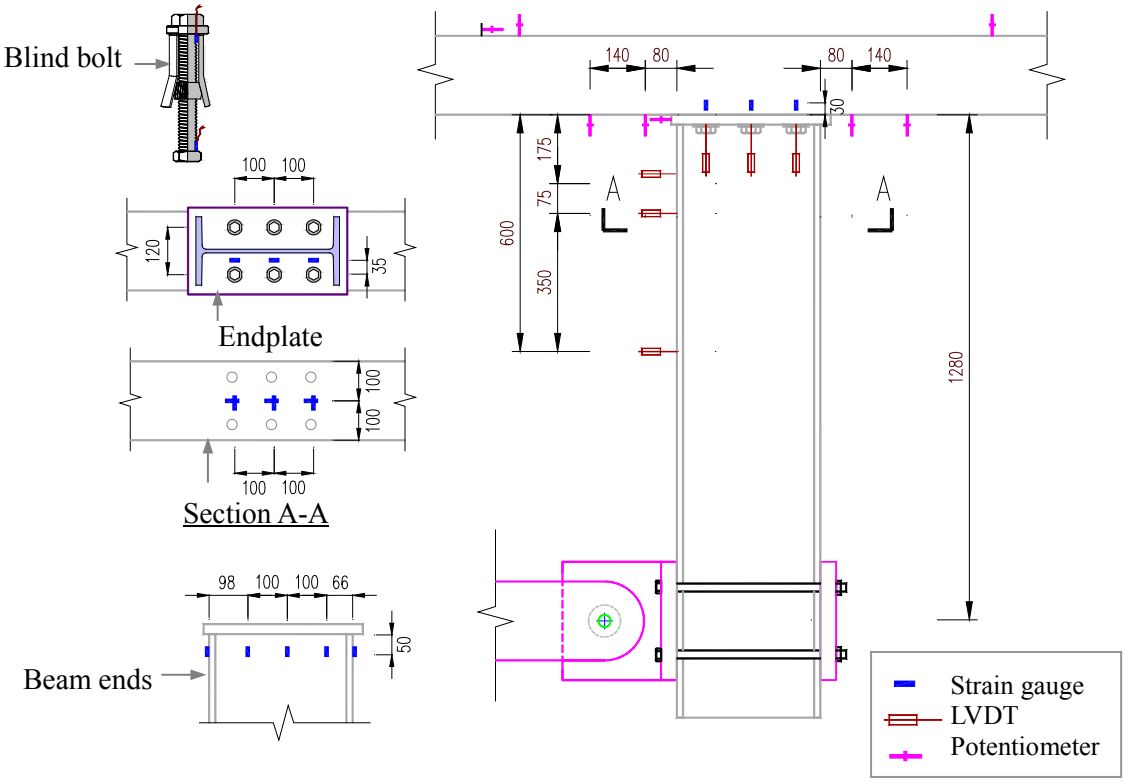

Figure 2. Configuration of the connections.

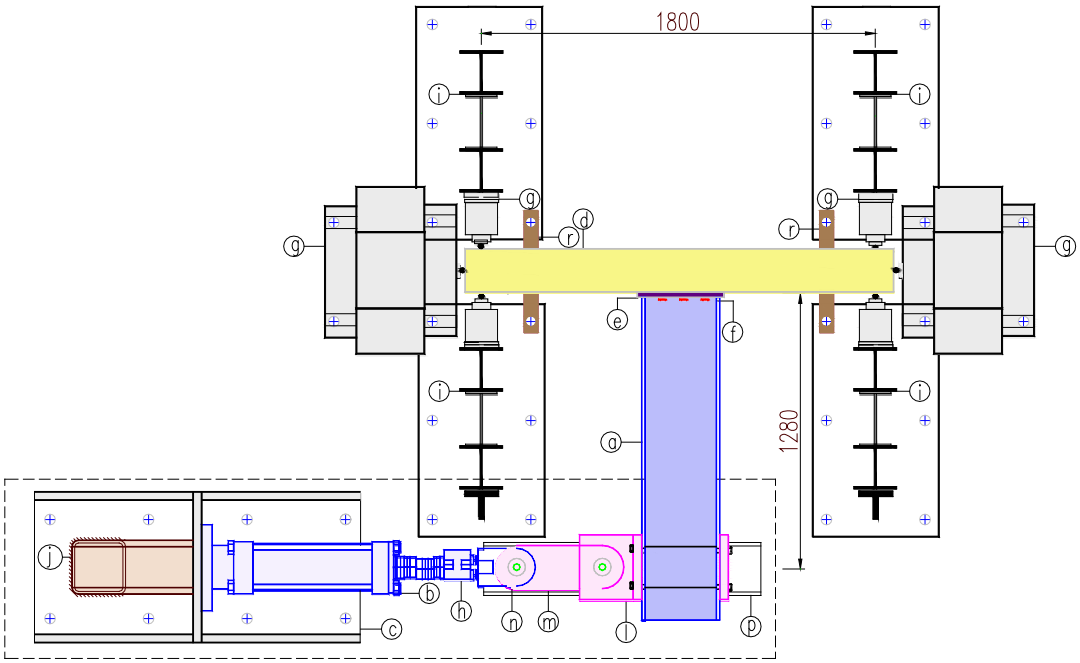

(a) Plan view

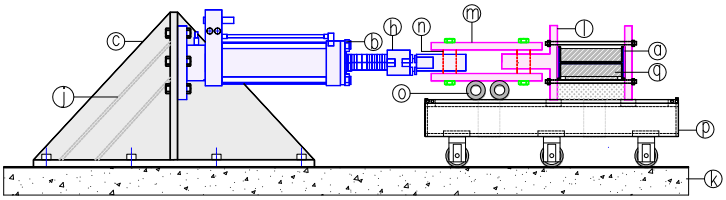

(b) Elevation view

a Test steel beam	g Lateral & end block	m Rigid link
b Horizontal actuator	h Load cell	n Link roller: rotation
c Reaction buttress	i Frame column	o Link roller: translation
d Test CFT column	j Brace	p Sliding base
e Test endplate	k Strong floor	q Local support & packing
f Blind bolts	l Head cap	r Out-of-plane restraint & tie-downs

Figure 3. Schematic of test-setup

Figure 4. Picture of test arrangement (top view).

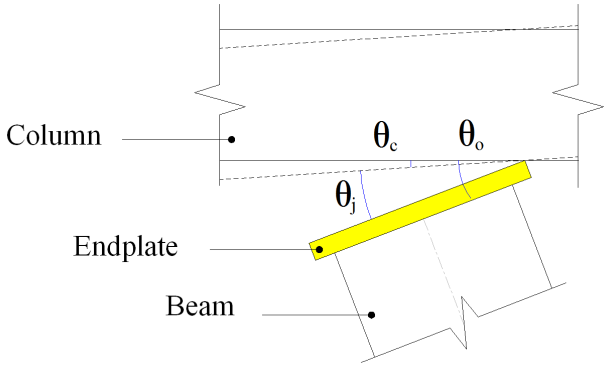

Figure 5. Schematic graph of joint rotation relationships.

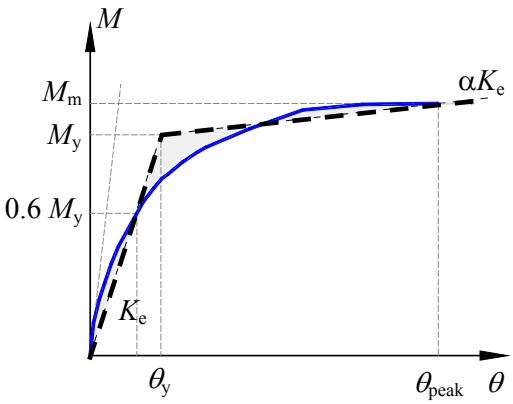

Figure 6. Definition of the yield point of the connection [22]

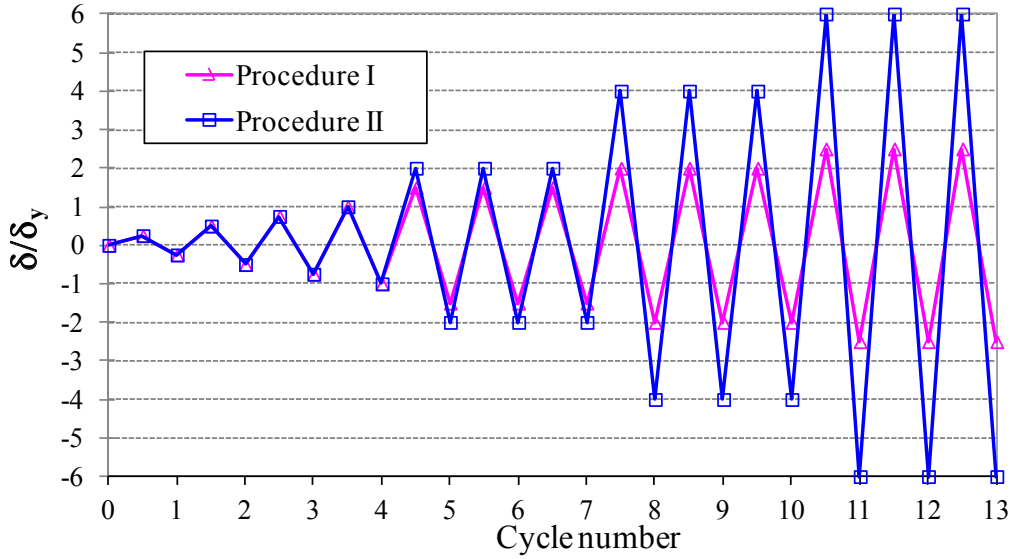

Figure 7. Illustration of the ECCS cyclic loading procedures [23]

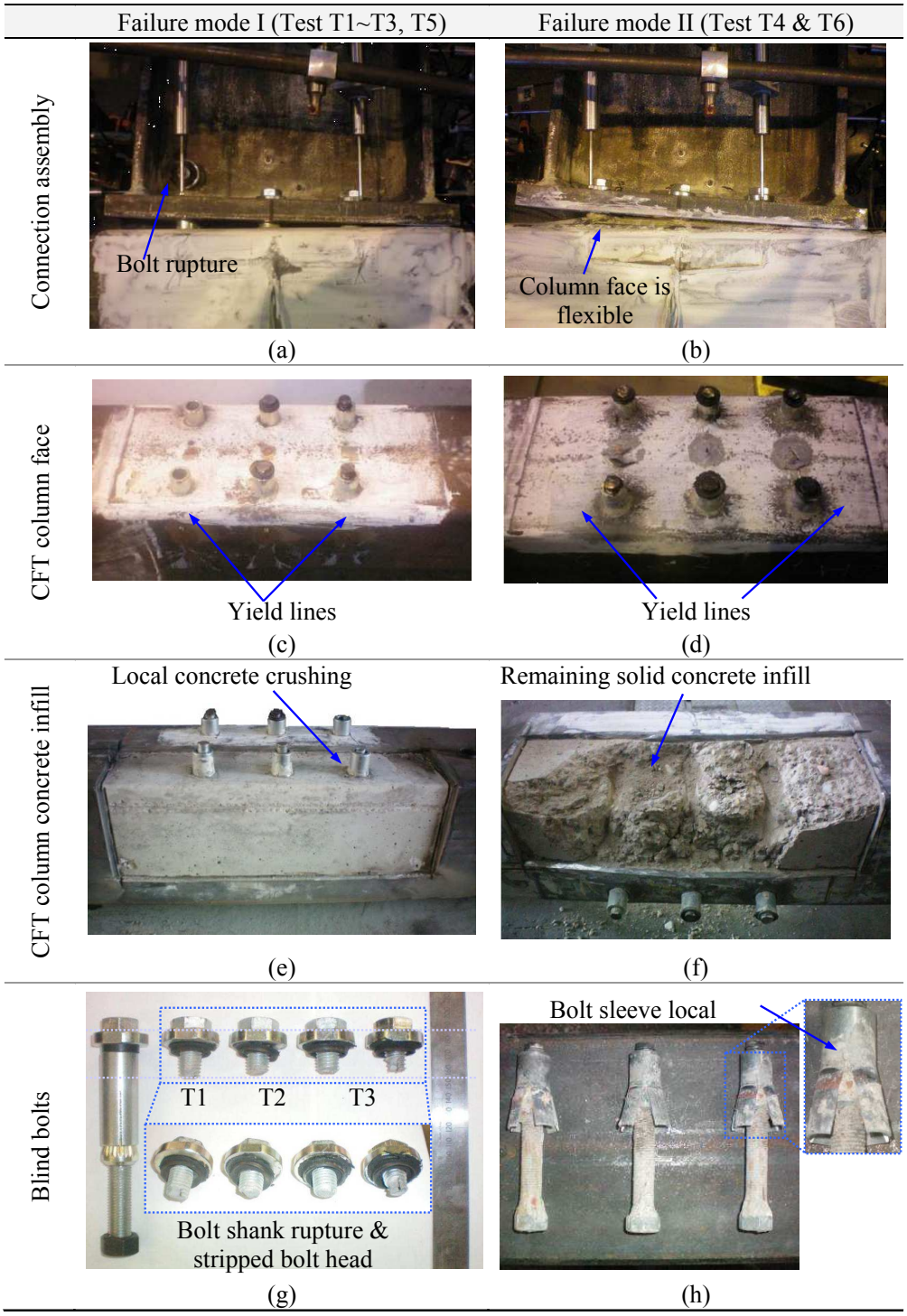

Figure 8. Representative failure modes of the connections.

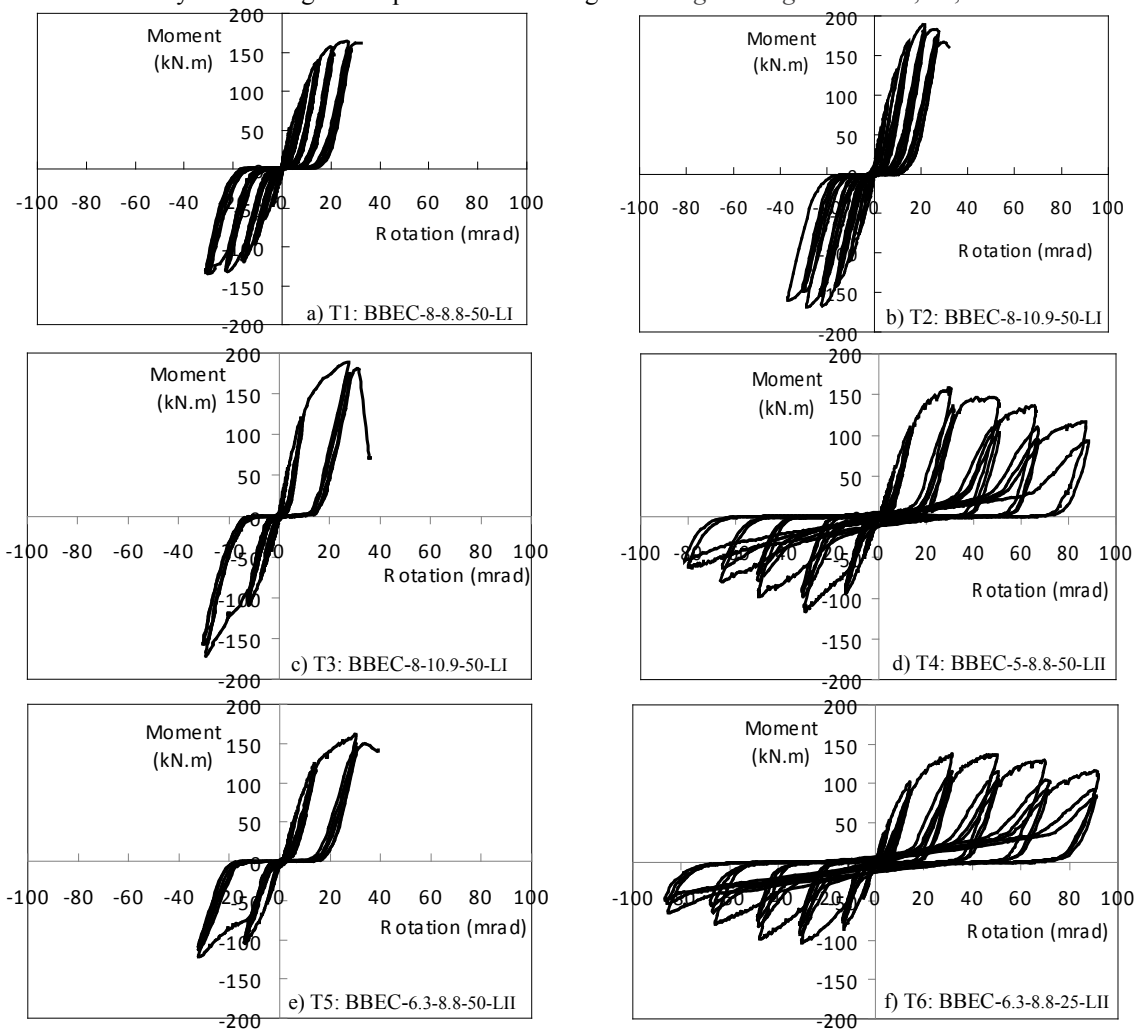

Figure 9. Hysteretic moment - rotation curves for test specimens.

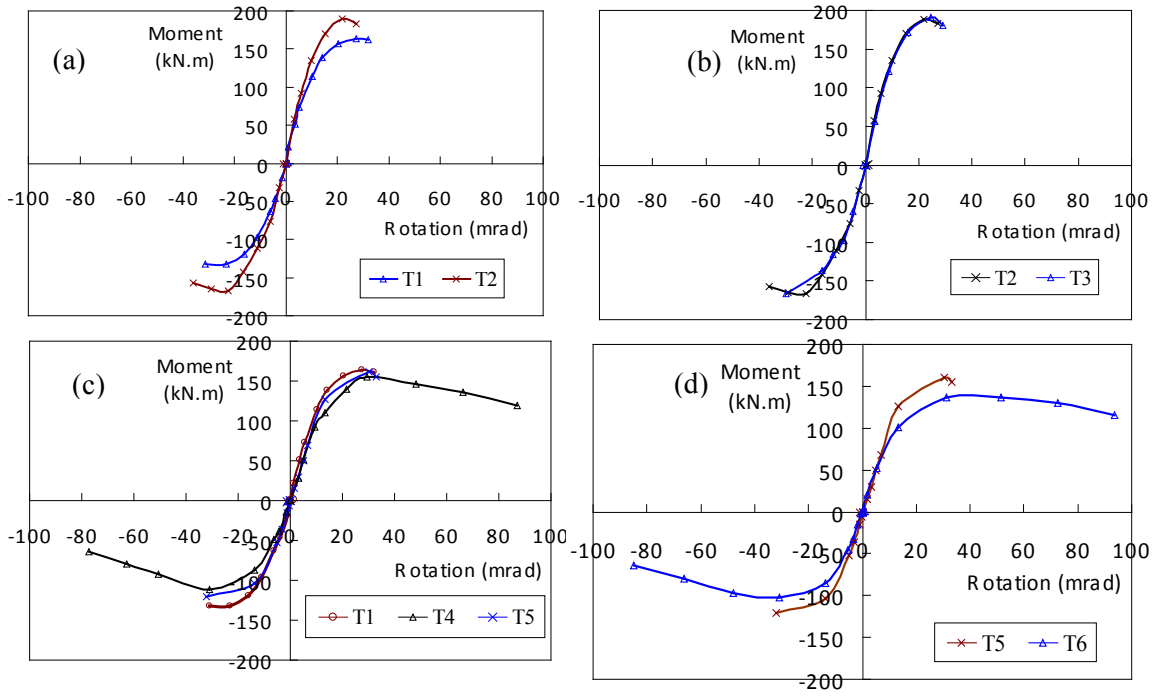

Figure 10. Comparison of moment-rotation hysteresis envelope curve.

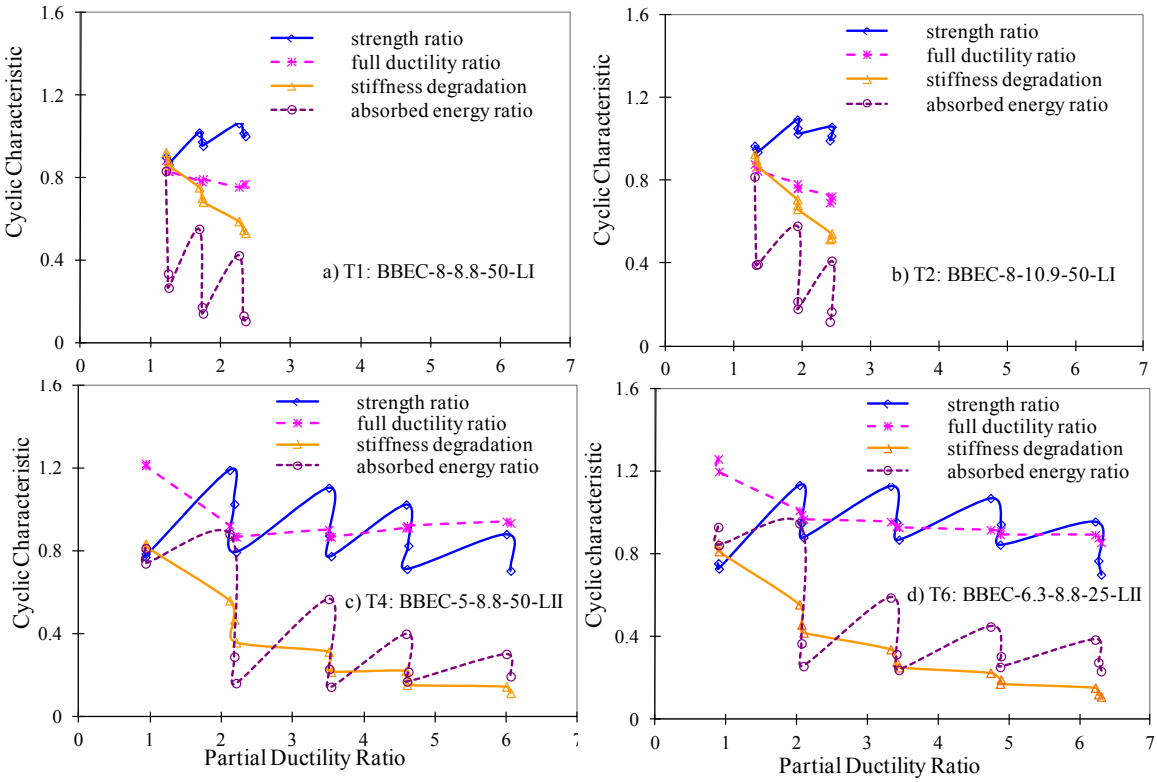

Figure 11. Cyclic characteristic ratios versus partial ductility ratio for positive excursions.